Glass-ionomer dental restorative

Part I: *a structural study*

K. A. MILNE[1], N. J. CALOS[1,2], J. H. O'DONNELL[1,†], C. H. L. KENNARD[1], S. VEGA[3], D. MARKS[3]
[1] *Department of Chemistry, The University of Queensland, Brisbane, Qld 4072, Australia*
[2] *The Centre for Microscopy and Microanalysis, The University of Queensland, Brisbane, Qld 4072, Australia*
[3] *Department of Chemical Physics, The Weizmann Institute, Rehovot 76100, Israel*

A structural study of glass-ionomer cement (GIC) dental restoratives has been completed. Transmission electron microscopy, selected area electron diffraction, and X-ray diffraction studies indicate domain-like microstructure in a new experimental material, whereas a featureless amorphous gel-like microstructure exists in the conventional GIC. Nuclear magnetic resonance studies were also conducted. The new experimental GIC contains domains of (i) bonelike material (apatite), (ii) mesoporous material and (iii) other framework structures (aluminium phosphate in the high cristobalite structure), with its setting chemistry a restructuring of the aluminosilicate glass around the template of poly(acrylic acid). Conventional glass-ionomer cement may set by a similar but slower process. Leaching properties of glass-ionomer cements are also explained.

1. Introduction

Glass-ionomer cement (GIC) has found growing use as a dental restorative [1]. GIC, first developed by Wilson and Crisp [2], introduced commercially by McLean [1] and described in detail by Mount [3], has high biological compatibility, but is brittle, with low fracture toughness. GICs also need precise stoichiometry for reaction and long setting times are common. However, leaching of fluoride ions from GIC, although not yet well understood [4], is convenient from a therapeutic point of view. One approach to developing an improved GIC lies in an examination of how these properties may be improved. At the present time, applications of GIC as a replacement for mercury amalgam dental restorative are limited by the mechanical weakness of GIC in comparison with amalgam. However, reinforced GIC with improved mechanical properties has been developed [5, 6] using poly(acrylic acid) (PAA) condensed with an active glass in the presence of an accelerator. The mechanical properties are improved further by incorporating fillers of glass fibre and glass particulate.

The term ionomer applies to polymeric substances which exhibit domains of ionic character, in a matrix of non-ionic character. Although named glass-ionomer cements, there is evidence [7] that the structure of GIC does not exhibit the properties of a true ionomer. Wilson and Nicholson [8] give a thorough historical review of studies of the structure and composition of GIC, and more recently, a communication [9] concludes that some of the glass dissolves, allowing secondary cement-forming reactions that contribute to hardening, i.e. the formation of silica gel, and if phosphate is present, aluminium phosphate gel. In the present work, the application of microstructural analysis techniques such as X-ray diffraction (XRD), nuclear magnetic resonance (NMR) and transmission electron microscopy (TEM) with selected area electron diffraction (SAED) not only confirms these conclusions but allows an understanding of the setting reaction.

2. Materials and methods

Experimental glass-ionomer cements were made from a glass of similar composition to G338 [10] (Table I). Poly(acrylic acid) (PAA), of molecular weight 5×10^6 Daltons, was dissolved (15% w/v) in deionized water, dried at 60 °C and ground in a ringmill for approximately 1 h. The dry polymer powder was mixed with the powdered glass (5 and 20% w/w polymer : glass). The resultant dry mixture was then mixed with either deionized water or the accelerator (1 g of powder to 0.6 ml of liquid). The accelerator was 40% v/v concentrated orthophosphoric acid (BDH) in deionized water. Setting occurred in approximately 3 min at room temperature. Four types of samples were studied as follows: sample A is glass powder alone; sample B is glass + accelerator; sample C is glass + PAA, set using deionized water; sample D is glass + accelerator + PAA. If present, the PAA concentration is 5% w/w polymer : glass unless otherwise stated. For some NMR experiments, a PAA concentration of

†Deceased 29th April 1995

0957–4530

TABLE I Glass compostion (mol %)

	Experimental glass[a]	G338 [10]
SiO_2	29	39.05
Al_2O_3	12	13.13
CaF_2	13	15.45
Na_3AlF_6	6	8.61
$AlPO_4$	33	18.66
AlF_3	7	5.10

[a] Electron microprobe analysis

20% w/w polymer:glass is used (stated in text). The samples could be moulded to shapes required for the respective experiments, or allowed to set and pulverized. The effects of humidity on GIC properties necessitated the study of well-set material dried by allowing it to stand open to the air at room temperature for at least a week. Powder X-ray diffraction (XRD) data were collected with Siemens D5000 and Philips PW1050 diffractometers with graphite monochromator using CuK_α radiation. Data were collected in the range of $2^\circ < 2\theta < 90^\circ$ in 0.05° steps. Specimens were annealed at 930 °C for 2 h to produce sharpened XRD patterns due to the improved crystallinity. Nuclear magnetic resonance (NMR) was performed on a custombuilt 200 MHz solid state spectrometer using cross polarization magic angle spinning (CP-MASS) for ^{13}C and a single 90° pulse for ^{2}H. Adamantane was the external standard for ^{13}C NMR spectroscopy and tetramethylsilane (TMS) the chemical shift reference. Transmission electron microscopy (TEM) and selected area electron diffraction (SAED) were performed on a JEOL JEM 4000 FX electron microscope operating at 400 keV. Electron microprobe analyses were performed on a JEOL JXA 8800L electron probe microanalyser operating at 15 kV.

3. Results

X-ray diffraction (XRD) patterns are shown in Fig. 1 and transmission electron micrographs (TEM) are given in Figs 2 and 3. The XRD patterns of the glass (sample A) (Fig. 1a) contain no sharp peaks, and confirm (i) the absence of large crystals and (ii) a non-periodic structure on the macroscopic scale (Table I). However, TEM studies (Fig. 2a) show that the glass is homogeneously cryptocrystalline consisting of numerous aggregated spheroids of the order of 10 nm in diameter. The XRD pattern of the annealed glass (Fig. 1b) closely matches cristobalite- (or $AlPO_4$) and apatite-type structures in solid solution.

The glass + accelerator (sample B) (Fig. 1a) does not show sharp peaks in the XRD analysis, indicating predominantly amorphous material. TEM (Fig. 2b) confirms a predominantly amorphous matrix, but the material contains large acicular (needle-like) crystals ~10 μm long and up to 1 μm thick. The material is a composite of large crystals in a porous and friable

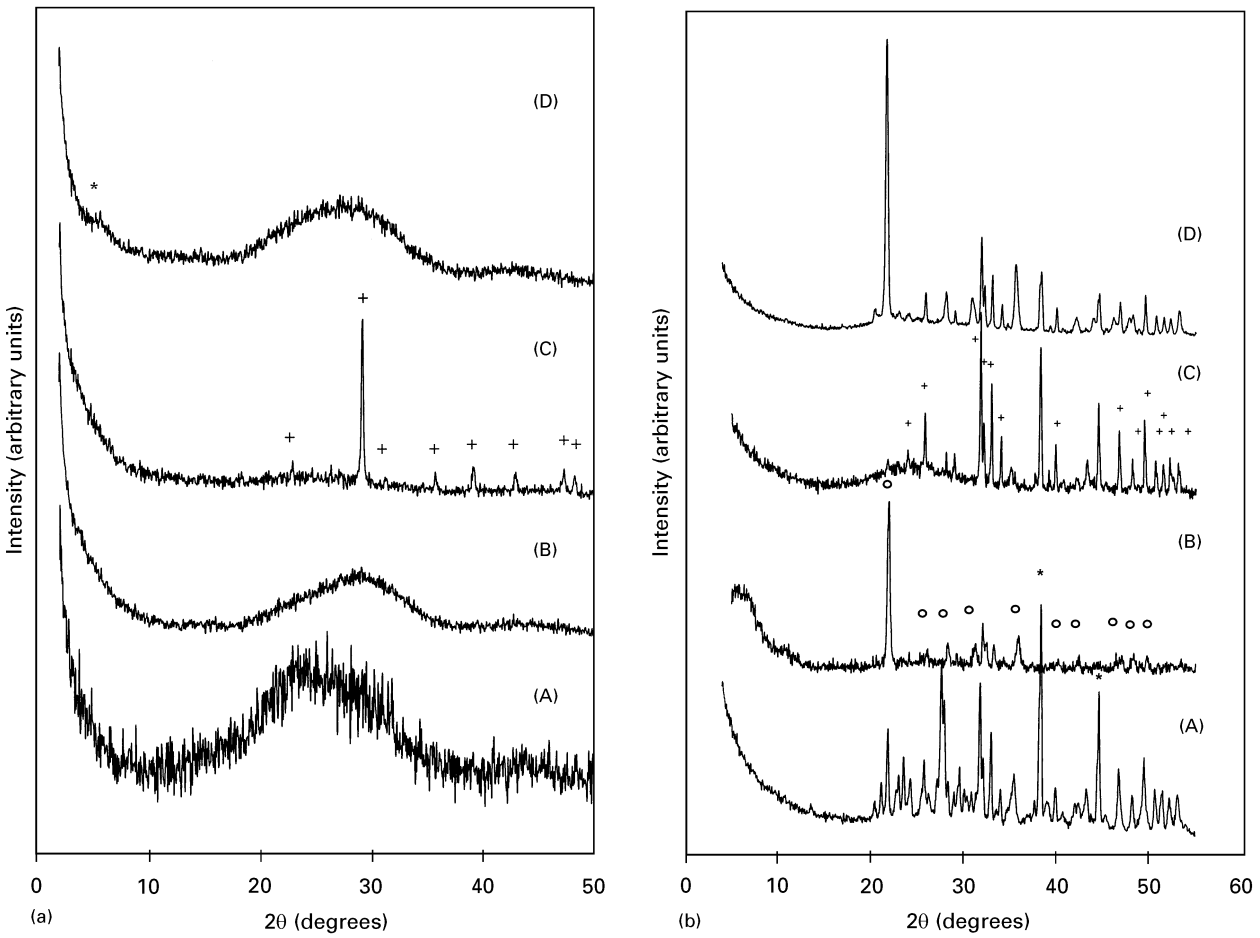

Figure 1 XRD traces of (a) unannealed GIC materials, (b) annealed GIC materials: (A) glass; (B) glass + accelerator; (C) glass + PAA; (D) glass + accelerator + PAA. (a) * mesoporous; + calcite; (b) * Al; + apatite, ○ cristobalite.

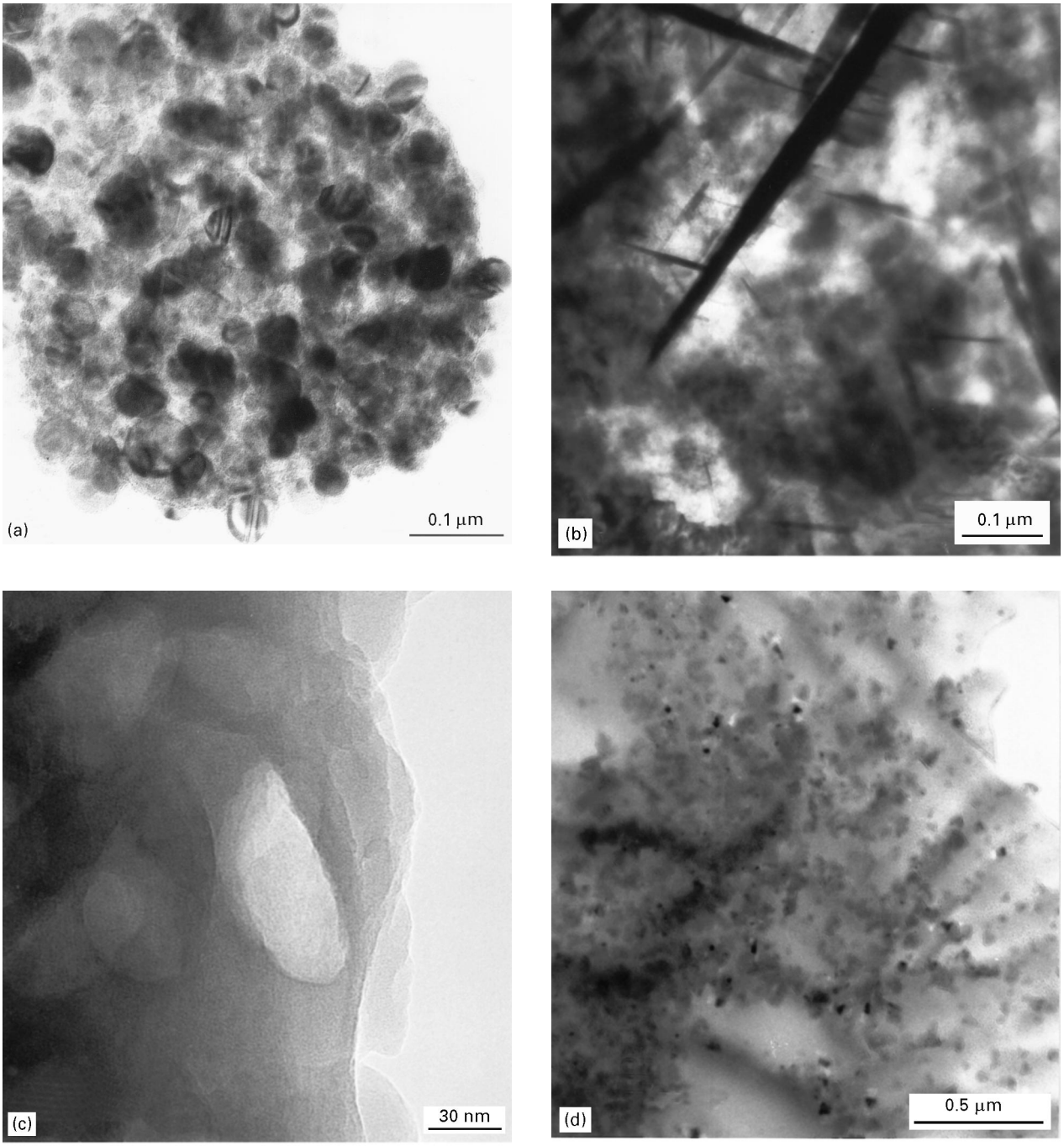

Figure 2 Electron micrographs of (a) glass, (b) glass + H_3PO_4, (c) glass + PAA, (d) glass + H_3PO_4 + PAA.

matrix. Since the volume fraction of the large crystals is not significant, there is no observable XRD line pattern (Fig. 1a). The XRD pattern of the annealed material (Fig. 1b) matches that of cristobalite-type structure.

Calcium carbonate (calcite) is also identified by XRD in the glass + PAA (sample C) (Fig. 1a). A minor amount of featureless scattering intensity is evident in the XRD trace in the region of $2\theta = 22–32^\circ$, characteristic of the amorphous matrix. The annealed glass + PAA (Fig. 1b), like the annealed glass, reveals a mixture of apatite with a minor amount of cristobalite-type structure. TEM (Fig. 2c) analysis shows the unannealed matrix to be homogeneous and amorphous, with no evidence of crystalline fringes or diffraction, in contrast to the glass alone. The crystalline pattern in the XRD is consistent with large crystals of calcite which were not identified in the TEM study.

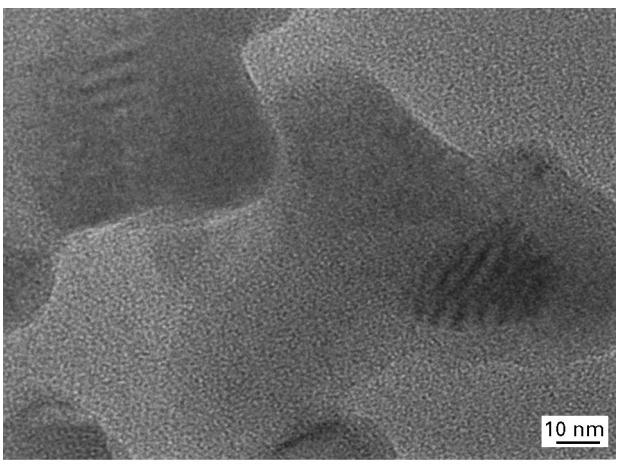

Figure 3 Electron micrograph of the domain structure of glass + H_3PO_4 + PAA.

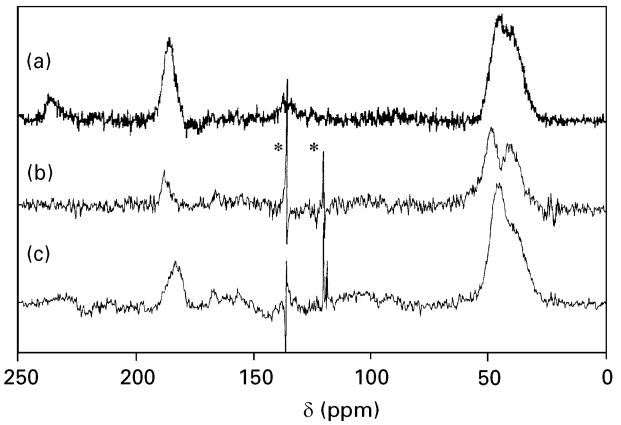

Figure 4 CP-MASS ^{13}C NMR spectra of (a) PAA, (b) glass + 20% PAA, (c) glass + H_3PO_4 + PAA. Probe breakthrough is indicated by asterisks.

The XRD pattern of glass + PAA + accelerator (sample D) (Fig. 1a) is also a broad amorphous pattern, with additional scattering at $2\theta = 2$–6°, attributed to mesoporous material. Annealing the glass + PAA + accelerator at 930 °C (Fig. 1b), produced a mixture of significant amounts of cristobalite and apatite. TEM (Figs 2d and 3) shows domains of phase contrasted material which exhibits crystallinity. The crystalline domains, observed only in sample D type material are integrally associated with a lighter phase material which exhibits amorphous character. Fig. 3 is a high resolution TEM image of the glass + PAA + accelerator (sample D) showing the crystalline domains more clearly. Lattice fringes are visible in the crystalline domains.

Fig. 4 shows the ^{13}C CP-MASS NMR spectra obtained for PAA, glass + PAA, and glass + PAA + accelerator. In each case, three peaks are observed, corresponding to the carboxyl signal at around 125 ppm and the α- and β-carbon signals at around 42 ppm, with the α-carbon peak occurring at the higher chemical shift. A summary of the NMR parameters is presented in Table II.

^{2}H MASS NMR spectra were obtained for glass + accelerator (sample B), glass + PAA (sample C), glass + PAA + accelerator (sample D, PAA 5%), and glass + PAA + accelerator (sample D, PAA 20%) (Fig. 5). The NMR signal for each of these materials is a single peak for which width, shape and nuclear relaxation time vary with composition. Table III is a summary of the lineshape information obtained from the spectrum shown in Fig. 5.

The ^{2}H MASS NMR spectrum for the glass + accelerator shows distinct spinning sidebands. A simulation of these experimental results is given in Fig. 5e (inset) based on an electric field gradient (EFG) tensor of (14.95, 45.06, −60.00) kHz. The strong central peak which in practice arises from the mobile (isotropic) fraction of the sample has been neglected. With increasing PAA content in the mixtures, these spinning sidebands are more difficult to resolve.

TABLE III ^{2}H nuclear magnetic resonance parameters

Sample	FWHM (Hz)	T_1 (ms)
Glass + accelerator	1700	–*
Glass + PAA	200	20
Glass + accelerator + PAA (5%)	1569	5.8*
Glass + accelerator + PAA (20%)	1117	5.6*

*Spinning sidebands observed.

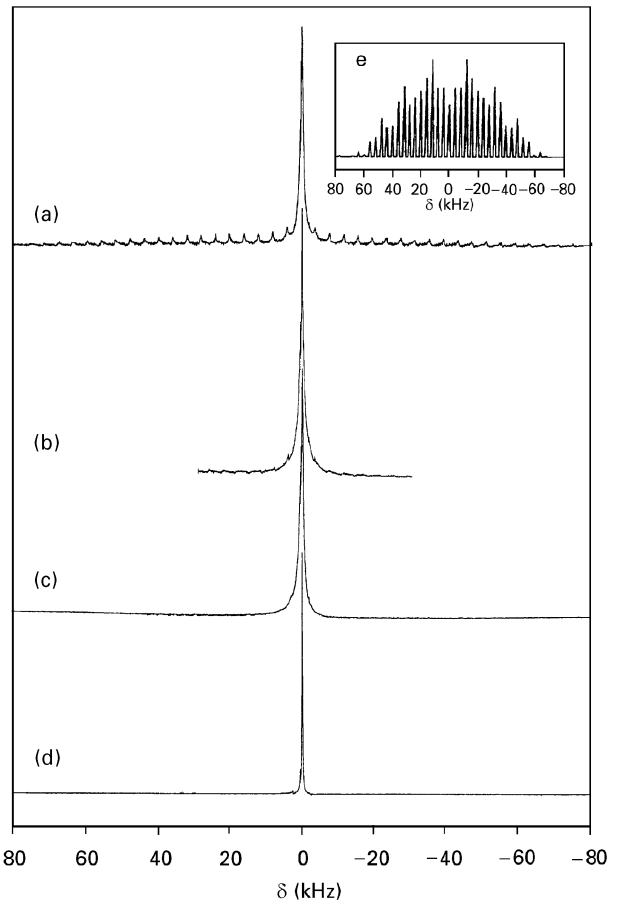

Figure 5 ^{2}H MASS NMR spectra of (a) glass + H_3PO_4, (b) glass + H_3PO_4 + 5% PAA, (c) glass + H_3PO_4 + 20% PAA, (d) glass + PAA, (e) simulation of spin sidebands of spectrum (a).

TABLE II CP MASS ^{13}C nuclear magnetic resonance parameters (TMS reference)

Sample	–CO_2–			α–C–			β–C–		
	δ (ppm)	FWHM (Hz)	I	δ (ppm)	FWHM (Hz)	I	δ (ppm)	FWHM (Hz)	I
PAA	181	359	35	44	767	100	–	–	–
Glass + PAA	188	194	26	49	229	82	42	695	100
Glass + PAA + accelerator	183	352	19	44	694	100	–	–	–

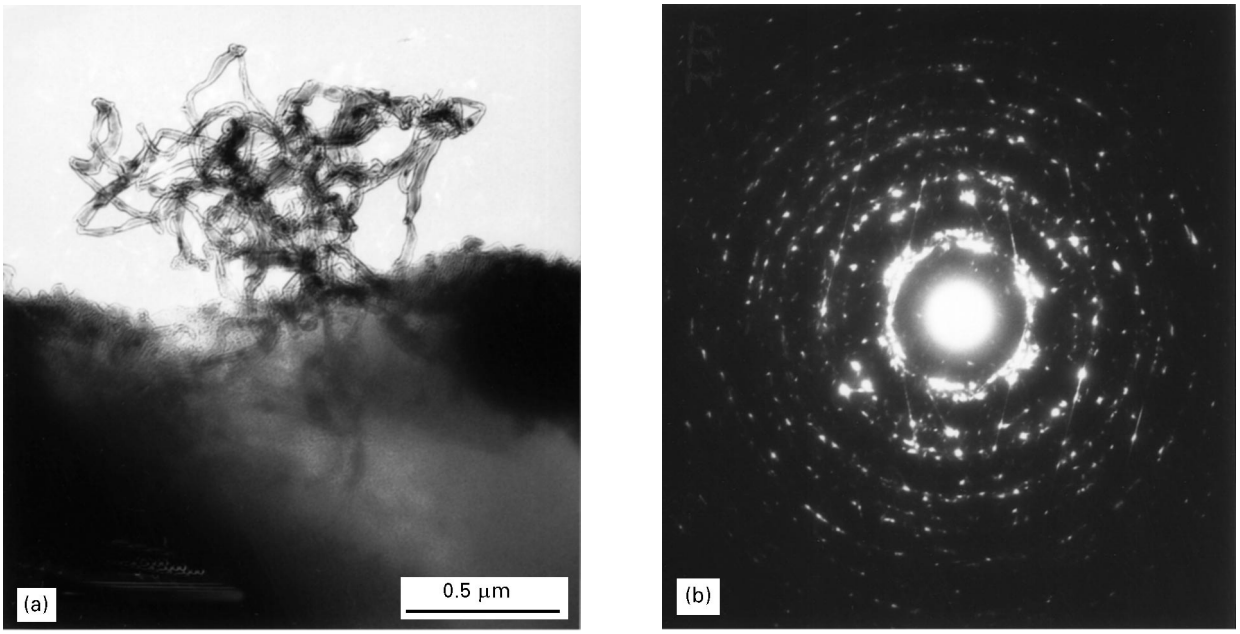

Figure 6 (a) Electron micrograph of polymer fibrils in inorganic matrix; (b) SAED pattern of area shown in Fig. 6a.

Fig. 6a is a high resolution TEM image of the glass + accelerator + PAA (sample D, ion mill thinned) showing fibrils extending from the matrix. The fibrils appear to extend into, and admix with, the matrix. The SAED pattern (Fig. 6b) of the area surrounding and including the fibrils shows streaks, together with a ring and spot pattern. Thus, the observed pattern may be interpreted as an overlay of patterns from (i) the fibrils and (ii) the host matrix. The fibril diffraction overlaps at several points with the diffraction from the host lattice. Therefore, the fibril structure at some point has the same diffraction characteristic as a crystal from the host lattice.

4. Discussion

The existing model [8] for the setting reaction of GIC's invokes extraction of metal ions from the outer layers of glass which remains essentially unreacted, and the formation of polyacrylate salts to give a gel. The hypothesis is made that a "siliceous hydrogel" coats unreacted glass particles. In some cases, an aluminium phosphate gel is formed. The model [8] suggests that glass particles are "glued" together with a polymer gel formed by the interaction between the polymer and the glass surface. In the present work, the results indicate a more extensive reaction with dissolution of glass and formation of new structures by recrystallization.

4.1. TEM

The TEM images (Figs 2 and 3) indicate that the microstructure of the matrix varies with the composition of the sample. The results indicate (Wilson [9]) cement-forming reactions with dissolution of the glass to form an amorphous gel which in time recrystallizes. However, the directionality of the lattice fringes in Fig. 3 (arrowed), together with the appearance of mesoporous material only when PAA is present, indicates that when the accelerator is used, it promotes recrystallization with templating around the polymer. Aluminium phosphate has been found to be present (cf. [9]).

4.2. ^{13}C NMR

The ^{13}C glass + PAA + accelerator (sample D) NMR spectrum (Fig. 4) is broad with unresolvable peak overlap which may be due to structural disorder and fast relaxation of the nuclei. For glass + PAA (sample C), and for glass + PAA + accelerator (sample D), the β-carbon peaks are broad, indicating a polymer with variable conformation in the solid. The PAA acid group in the glass + PAA (sample C) may be more mobile than in the glass + PAA + accelerator (sample D), as it is free to move in a disordered and unstrained environment since there is little phosphate present to condense the aluminosilicate ions into framework structures. In the glass + PAA + accelerator, the acid group may be locked within a framework structure giving generally broader peaks. The weaker carbonyl peak for glass + PAA (sample C) compared to glass + PAA + accelerator (sample D) confirms the restriction of the acid group. Alternatively, the restricted PAA acid group may be involved in coordination to aluminium ions rather than involved in hydrogen bonding. These two models provide strong relaxation mechanisms for the carbon nucleus, giving smaller NMR peaks.

Diffusional mobility may be responsible for the narrowing in the proton-decoupled ^{13}C spectrum of the PAA in the glass + PAA, similar to the line-breadth effects in ^{13}C spectra observed by Nagy *et al.* [11]. In each sample, the carbonyl peak is also sharp. In the glass + PAA spectrum, the mobility is consistent with the high mobility in the ^{2}H NMR lineshape study (Section 4.3). The breadth of each ^{13}C signal indicates that the mobility of the PAA increases with PAA content. The polymer itself is changing its own

environment. The α-carbon in particular is either immobile or has greater torsional variation. Where long-range order is found, the polymer is constrained in its environment and away from the influence of other polymer molecules. The analogous study when formic acid is adsorbed onto zeolite Y [12], shows deshielding and sharpening of the carbonyl signal consistent with complex formation, possibly with calcium or aluminium ions, which decrease the polymer mobility. Alternatively, the sharpening and loss of intensity of the carbonyl peaks in the glass + PAA may be attributed to decarboxylation of PAA (possibly due to the Brønsted acidity of the aluminium in the glass) similar to the decomposition of formic acid in ultra-stable H–Y zeolite [12]. This decarboxylation is consistent with the observation of calcite in the XRD trace of glass + PAA.

4.3. ^{2}H NMR

Deuterium NMR supports these conclusions. Fig. 5e shows the expanded simulated sideband pattern which matches the solid state component of the observed total spectrum. However, the total experimental spectrum (Fig. 5a) illustrates the relative proportions of the freely rotating deuterium to solid state deuterium in the sample. The centre line is thus due to a mobile fraction and the sideband pattern to a less or immobile fraction of the sample. The width of the envelope of spinning sidebands gives information on the anisotropy of deuterium mobility within the material. In the samples containing phosphate, a fraction of the deuterium appears to be constrained. However, as the PAA content of the cement is increased, the fraction of sample giving rise to spinning sidebands decreases. Therefore, the mobility of the deuterium within the GIC is directly related to the polymer content. The spin-lattice relaxation time (T_1) also indicates ordering of the H bonds. Short relaxation times occur when distinct mechanisms for relaxation exist in a well-ordered crystalline framework.

In the present study, increasing the PAA content of the cements gave sharper DMR peaks and the loss of spinning sidebands. Glass reacted with PAA only (sample C) gives the sharpest peak with $T_1 = 20$ ms, whereas glass + PAA + H_3PO_4 (sample D) has $T_1 \sim 5.7$ ms, and glass + H_3PO_4 (sample B) showed $T_1 < 5.6$ ms. These observations are consistent with phosphoric acid promoting network formation in the aluminate–silicate–phosphate matrix, whereas the PAA promotes the existence of relatively easily diffusible, isolated aluminate, silicate and phosphate ions. Annealing experiments have shown the increased proportion of cristobalite structure in glass + H_3PO_4 (sample B), whereas the non-framework compound with the open ionic apatite structure results from annealing glass + PAA (sample C).

In a constrained system (i.e. where atoms are more rigidly bound, or atomic motion is anisotropic) the EFG tensor is large. This EFG tensor decreases with mobility of the nucleus concerned, since if the nucleus can move, then the motional average of the EFG tensor will be less than if the nucleus were forced to experience its full effects. The breadth of the envelope of spinning sidebands decreases as the magnitude of the EFG tensor decreases, so that the lineshape of the ^{2}H signal is an indicator of the anisotropy of the hydrogen environment.

Using lineshape analysis demonstrated by Kustanovich *et al.* [13], the ^{2}H in the glass + H_3PO_4 (sample B) undergoes rapid restricted rotational motion about a fixed site. Therefore, this material has a hydrogen bonded network, whereas in the glass + PAA (sample C), the ^{2}H has unrestricted rapid rotational and translational motion within a poorly ordered matrix. Interestingly, when the samples were made with D_2O, they did not set rigidly, but to a rubbery consistency which did not harden with time. A similar effect is seen when mineral acids (non-deuterated) are used. Therefore, rigid setting apparently requires the presence of hydrogen atoms or ions and condensible phosphate ions.

In the glass + accelerator + PAA (sample D), the accelerator (phosphoric acid) produces structures where H atoms are bound in extensive H-bonded networks. Without the accelerator, the amorphous material gives the deuterium relatively long spin-lattice relaxation times and therefore, sharp signals with no spinning sidebands. A decrease in the ordered hydrogen bonding was seen with increasing PAA content.

Both the ^{13}C and ^{2}H NMR show a range of mobilities which may be accounted for by the existence of an ordered, hydrogen-bonded network formed on addition of H_3PO_4 to the reaction mixture. PAA has the opposite effect, i.e. structure-breaking, giving rise to a free, ionic, disordered state in the GIC matrix. A strong endothermic reaction observed during the setting of the cements containing PAA supports the structure-breaking hypothesis.

When both the PAA and the H_3PO_4 are present, the opposite effects combine to produce an intermediate material where the mobility of the ^{13}C increases with PAA content and domains of ordered, hydrogen bonded networks or framework compounds coexist with amorphous material where the ^{13}C mobility is higher. This interpretation is consistent with the domains observed in TEM (Figs 2 and 3). More detailed investigations, e.g. ^{13}C–^{1}H magnetization transfer determinations, are required in order to determine the disposition of the PAA in relation to the inorganic matrix.

4.4. Polymer incorporation

Evidence for polymer incorporation is shown by TEM in Fig. 6a. Polymer fibrils are observed in part of the ion mill thinned section used for high resolution TEM. The fibrils are seen to extend into the matrix of the material in an intimate mixture of polymer and set matrix. The fibrils are probably ordered because they give SAED streaks (see Fig. 6b) which coincide with matrix diffraction spots indicating some coherence with the host structure. There are apparently common points in the guest/host structures, i.e. orientational relationships, consistent with the template hypothesis.

4.5. The setting reaction

The setting reaction is a function of water concentration. Too much water, i.e. when a hardening restoration is not protected from saliva, prevents the cement from setting, but too little water causes the cement to dry out and become brittle. A possible mechanism is that the water is involved in anchoring the polymer to the aluminosilicate structure. Addition of the accelerator may speed up this process and cause faster rigid setting. Even though it appears that protons are necessary for rigid setting, it is most probable that condensible phosphate ions are also necessary. Without the accelerator, rigidity develops slowly, and is a possible explanation for continued hardening of GIC for up to six months after application. The glass + PAA set initially to a rubbery consistency, then endothermically to a rigid entity. This long-term hardening appears if a minimum amount of water is present, as in saliva, but does not happen in the absence of water. As discussed above, the slow rubbery setting reaction happened when deuterated samples were made for NMR. However, the deuterated samples did not harden with time. A possible reason for the endothermic hardening reaction is the uncoiling of the polymer as the crystallization proceeds, forcing the aluminosilicate matrix into a templated structure with an increase in volume. In heavy water (D_2O) experiments, the carboxylic acid groups of the PAA would be less ionized, owing to the lower dissociation rate of deuterium compared with hydrogen. Thus, the polymer would be more coiled and less available for complex formation. This control of the uncoiling of PAA is desirable because of minimization of shrinkage. Low shrinkage, or even expansion of the polymeric cement during setting, reduces the occurrence of fissures between the tooth and the cement, where bacteria and food residues may accumulate and cause decay.

4.6. Properties of GIC

XRD has shown that without the phosphoric acid, calcium carbonate is formed, possibly as a result of decarboxylation of a PAA–Ca complex or from carbon dioxide absorbed from the air reacting with Ca ions released at some stage of the setting. Either case explains why some conventional GICs are attacked by acid and dissolve. However, no calcium carbonate is found in the glass + accelerator + PAA (sample D) where phosphoric acid stabilizes the Ca^{2+} ion $[3Ca^{2+} + 2(PO_4^{3-}) \Rightarrow \text{insol. } Ca_3(PO_4)_2]$.

4.7. Mesoporous material

In the mouth, once set, the GIC takes on the colour of the surrounding teeth, absorbs and desorbs water as required, and leaches fluoride ions at a controlled rate. The presence of mesoporous material, detected by XRD, may help to explain these properties. The porous nature of the product means that it can reversibly take up water and ions and perhaps any other agents which determine tooth colour.

Mesoporous material was found only when the polymer was present. The production of mesoporous materials or zeolites by a templating process has been previously reported [14, 15], but the use of high polymers as templates has not been reported. The templating process may be considered as the polymer forcing a long-range structure on the recrystallizing aluminosilicate matrix. The evolution of heat on mixing of the glass and phosphoric acid indicates that there is a definite exothermic reaction between the glass and the accelerator to dissolve the glass. Then if PAA is present, another endothermic reaction forms the mesoporous material. XRD evidence shows that the mesoporous material is not formed when the PAA is not present. Neither is the endothermic reaction observed.

4.8. Domain structure

The observed domain structure (Fig. 3), where regions of crystallinity are interspersed with amorphous material is of interest in the design of strong materials. A stronger material is formed when there are a large number of small crystallites, giving compressive strength, embedded in a flexible amorphous matrix.

5. Conclusions

A new material consisting of domains of (i) apatite, (ii) mesoporous material and (iii) aluminium phosphate in an amorphous matrix has been observed in cements formed by reaction of GIC glass with PAA and orthophosphoric acid. This characterization is in contrast with the previous models of setting chemistry, in which the PAA essentially acts as an adsorbate to the aluminosilicate phase. Subsequently, a new model for the setting chemistry of glass-ionomer cements has been developed which explains their unusual behaviour with respect to water during and after setting, based upon participation of the PAA with the accelerator in an attack on the inorganic phase.

Acknowledgements

The authors thank The University of Queensland Foundation Ltd. for financial support; Professor Ian D. R. Mackinnon of the Centre of Microscopy and Microanalysis, The University of Queensland, for use of equipment, and discussion and advice in the preparation of the manuscript; Allied Colloids Australia Pty. Ltd. for supplying the poly(acrylic acid); Nulite Systems International Pty. Ltd. for supplying some materials; Lambert Bekessy, of the Department of Mining and Metallurgical Engineering, The University of Queensland for use of the X-ray diffractometer; Vladimir Ladizanski and Dov Grobgeld, Department of Chemical Physics, the Weizmann Institute, Israel for help in collecting the NMR data; Alan Todhunter, The Centre for Advanced Materials Technology, The University of Sydney, Australia for helpful discussion; John P. Gage, Department of Dentistry, The University of Queensland for clinical advice; The Australian National Beamline Facility and the

Australian Nuclear Science and Technology Organization for travel funding for NJC; NJC extends gratitude to Liora and Oren Bogin for invaluable assistance in the course of this study.

References

1. J. W. McLEAN, in "An atlas of glass-ionomer cements: a clinician's guide", edited by G. J. Mount (Martin Dunitz Ltd., London, 1990), foreword.
2. A. D. WILSON and S. CRISP, British Patent No. 1,422,337 (1972).
3. G. J. MOUNT, "An atlas of glass-ionomer cements: a clinician's guide" (Martin Dunitz Ltd., London, 1990), preface.
4. S. CRISP and A. D. WILSON, *J. Dent. Res.* **53** (1974) 1420.
5. K. A. MILNE and A. J. TODHUNTER, Provisional Australian Patent Application No. PL8243 (1993).
6. T. BREMNER, K. A. MILNE, J. H. O'DONNELL, A. J. TODHUNTER and A. K. WHITTAKER, Preprints of the 3rd Pacific Polymer Conference of the Pacific Polymer Federation, Gold Coast, Australia, 13–17 December (1993) p. 367.
7 E. A. WASSON and J. W. NICHOLSON, *J. Dent. Res.* **72** (1993) 481.
8. A. D. WILSON and J. W. NICHOLSON, In "Acid-base cements: their biomedical and industrial applications": Chemistry of Solid State Materials, Vol 3, edited A. R. West and H. Baxter (Cambridge University Press, Cambridge, 1993) Chapter 5.
9. A. D. WILSON, *J. Mater. Sci. Lett.* **15** (1996) 275.
10. D. WOOD and R. HILL, *Biomaterials* **12** (1991) 164.
11. J. B. NAGY, E. G. DEROUANE, H. A. RESING and G. R. MILLER, *J. Phys. Chem.* **87** (1983) 833.
12. T. M. DUNCAN and R. W. VAUGHAN, *J. Catal.* **67** (1981) 49.
13. I. KUSTANOVICH, D. FRAENKEL, Z. LUZ, S. VEGA and H. ZIMMERMAN, *J. Phys. Chem.* **92** (1988) 4134.
14. J. C. VARTULI, C. T. KRESGE, M. E. LEONOWICZ, A. S. CHU, S. B. McCULLEN, I. D. JOHNSON and E. W. SHEPPARD, *Chem. Mater.* **6** (1994) 2070.
15. J. S. BECK, J. C. VARTULI, G. J. KENNEDY, C. T. KRESGE, W. J. ROTH and S. E. SCHRAMM, *Chem. Mater.* **6** (1994) 1816.

Received 23 August
and accepted 18 September 1996